

LVVC: A Learned Versatile Video Coding Framework for Efficient Human-Machine Vision

Xihua Sheng, Li Li, *Member, IEEE*, Dong Liu, *Senior Member, IEEE*, and Houqiang Li, *Fellow, IEEE*

Abstract—Almost all digital videos are coded into compact representations before being transmitted. Such compact representations need to be decoded back to pixels before being displayed to human and – as usual – before being processed/analyzed by machine vision algorithms. For machine vision, it is more efficient at least conceptually, to process/analyze the coded representations directly without decoding them into pixels. Motivated by this concept, we propose a learned versatile video coding (LVVC) framework, which targets on learning compact representations to support both decoding and direct processing/analysis, thereby being versatile for both human and machine vision. Our LVVC framework has a feature-based compression loop, where one frame is encoded (resp. decoded) to intermediate features, and the intermediate features are referenced for encoding (resp. decoding) the following frames. Our proposed feature-based compression loop has two key technologies, one is feature-based temporal context mining, and the other is cross-domain motion encoder/decoder. With the LVVC framework, the intermediate features may be used to reconstruct videos, or be fed into different task networks. The LVVC framework is implemented and evaluated with video reconstruction, video processing, and video analysis tasks on the well-established benchmark datasets. The evaluation results demonstrate the compression efficiency of the proposed LVVC framework.

Index Terms—Deep neural network, human and machine vision, learned video coding, video processing, video analysis.

1 INTRODUCTION

VIDEOS contribute to 75% of all Internet traffic in 2017, and the percentage reached 82% in 2022. A digital video is composed of several frames with each frame as a static image. For a typical 1080p video in the standard dynamic range, 24 bits are used to represent the color (r, g, b) of each pixel, and the size of one frame can be approximated as 6Mbytes. For a video of 30 frames per second, the bit rate can be as high as 180Mbytes per second without compression. Therefore, encoding videos into compact representations with smaller sizes is an urgent requirement to reduce the transmission cost. After receiving the transmitted compact representations, they need to be decoded back to the pixel domain before being displayed to humans.

In addition to being decoded for display, the coded video representations are also needed to be processed/analyzed by machine vision algorithms in various video applications such as TV broadcasting and traffic monitoring. Video processing aims to improve video quality for a better human visual experience, such as reducing video noise and increasing video resolution. Video analysis refers to understanding the video scenes, such as recognizing dangerous human actions or detecting the appearance of target objects. To perform these machine vision algorithms, the coded representations usually need to be fully decoded back to pixels first. However, for machine vision, it is more efficient at least conceptually, to process/analyze the coded representations directly without decoding them into pixels.

Therefore, in this paper, our goal is to propose a video coding framework for efficient human-machine vision (VCHM). To make the proposed video coding framework versatile for both human and machine vision, we put forward three requirements for this framework, i.e., it should: 1) achieve high compression efficiency for video reconstruction and effective performance for human and machine vision tasks; 2) enable directly performing machine vision algorithms without decoding the coded representations into pixels; 3) be independent of the subsequent machine vision tasks. The first requirement is to make the framework reduce transmission and storage costs while keeping high reconstruction quality and task performance. The second requirement is to save more computational costs for machine vision tasks and improve real-time task processing. The third requirement is to make the framework general enough so that it can be applied to various tasks. Meeting all three requirements at the same time is extremely demanding and difficult. Existing solutions of VCHM are more or less unable to meet one or more of these requirements.

The existing solutions of VCHM can roughly be divided into three categories. Solutions in the first category focus on the compression of deep features of neural networks. Videos are firstly converted to features by the task networks on the front end. The features are packed into a video sequence and compressed by video codecs or directly compressed by feature codecs [1], [2] to compact representations. The compact representations are decoded into features and used by the task networks on the server end. Although this kind of solution can offload part of the computation from servers to front-end devices, their encoders can not meet the requirement to be independent of the subsequent machine vision tasks. It is difficult to make the compressed features general enough for different scenarios. In addition, when

- Date of current version Jan 18, 2023. (Corresponding author: Li Li).
- The authors are with the CAS Key Laboratory of Technology in Geo-Spatial Information Processing and Application System, University of Science and Technology of China, Hefei 230027, China (e-mail: xhsheng@mail.ustc.edu.cn; lil1@ustc.edu.cn; dongeliu@ustc.edu.cn; lihq@ustc.edu.cn).

the human further analysis is required, this kind of solution uses a generative model to reconstruct videos from the deep features [3]. However, the generated videos are of low quality, especially at high bit rates, which can not meet the requirement of high human visual experience.

Solutions in the second category explore to use a scalable bit stream [4], [5], [6] to support the hybrid human-machine vision. High-level features, such as the output of the task networks (class IDs and bounding boxes for objects) [5], [6], and low-level features, such as motion and content information of objects and background, are extracted and compressed separately. The bit streams of high-level features and low-level features are organized and combined into a scalable bit stream. Only part of the scalable bit stream needs to be transmitted and decoded depending on the machine vision tasks at the server end. This kind of solution still can not meet the requirement to be independent of the subsequent machine vision tasks. The extracted high-level features may not be general to various vision tasks. The encoder needs to be adjusted when applying this kind of solution to unseen vision tasks.

Solutions in the third category need to decode the bit stream back to pixels first and then perform machine vision algorithms. As illustrated in Fig. 1 (a), we refer to this kind of solution as *Reconstructing First, Processing Second* or *Reconstructing First, Analysis Second* paradigm. They compress the videos into bit streams using traditional video codecs, such as VTM (reference software of H.266/VVC). The bit stream is decompressed to the pixel domain and fed into the task networks. This kind of solution can achieve high compression efficiency for video reconstruction. However, it can not meet the requirement of directly performing machine vision tasks without decoding the bit stream into pixels. Some earlier learned video codecs [7], [8], [9] may have the potential to meet the requirement but their compression efficiency is inferior to the traditional video codecs. Recent conditional coding-based learned video codecs [10], [11], [12], [13], [14] rely on learning temporal contexts and have caught up with or even surpassed traditional video codecs towards compression efficiency under certain conditions. However, learning temporal contexts from previous frames makes their decoding highly coupled with video reconstruction. It is infeasible to apply them to video processing and video analysis tasks without fully decoding the bit stream to pixels.

To meet the above-mentioned three requirements at the same time, we propose a learned versatile video coding framework (LVVC). As illustrated in Fig. 1 (b), our proposed framework contains a feature-based compression loop and a task network. To make the feature-based compression loop decouple with the video reconstruction in the pixel domain, we propose two key technologies, one is feature-based temporal context mining, and the other is cross-domain motion encoder-decoder. In the feature-based compression loop, one frame is encoded (resp. decoded) to intermediate features, and the intermediate features are referenced for encoding (resp. decoding) the following frames. On the decoder side, the intermediate features may be used to reconstruct videos (pixels) or be fed into different task networks for various processing/analysis tasks, thereby being versatile for both human and machine vision. We evaluate

our framework on well-established benchmark datasets. The evaluation results demonstrate that the framework achieves comparable compression efficiency compared with the state-of-the-art video coding schemes, meanwhile supports different machine vision tasks efficiently in terms of both accuracy and computation.

Our contributions are summarized as follows:

- We propose a learned versatile video compression framework for efficient human-machine vision. The framework can achieve good performance for video reconstruction, video processing, and video analysis simultaneously.
- We propose a feature-based temporal context mining and a cross-domain motion encoder-decoder, which make our encoder and decoder decouple with the fully decoded video in the pixel domain.
- We propose to use the intermediate features rather than the fully decoded video in the pixel domain to perform various human-machine vision tasks, which can save much computational cost when video reconstruction is not required.

The remainder of this paper is organized as follows. Section 2 gives a brief review of related work. Section 3 introduces the overview of our framework. Section 4 and Section 5 describe the detailed network architectures and corresponding optimization methods. Section 6 and Section 7 present the experimental setup and experimental results of the framework. Section 8 analyzes the influence of proposed key technologies. Section 9 concludes this paper.

2 RELATED WORK

2.1 Video Coding for Hybrid Human-Machine Vision

Existing solutions of video coding for hybrid human-machine vision can be divided into three categories.

In the first category, solutions focus on feature compression. Features play an important role in machine vision tasks. In view of the necessity of transmitting compact descriptors of features, MPEG has finalized the standardization of compact descriptors for visual search (CDVS) (ISO/IEC15938-13) in Sep. 2015 [1] and compact descriptors for video analysis (CDVA) (ISO/IEC15938-15) [2] in July 2019 for efficient and effective image/video retrieval and analysis. With the deployment of learning-based applications, Chen et al. [15] proposed to compress the deep features of neural networks. However, even for machine vision tasks, further human analysis is required when the computer recognizes abnormal actions or detects the target object. These feature coding-based schemes only focus on feature compression while ignoring human visualization. Duan et al. [3] leveraged the generative models to reconstruct videos from features. However, the generated videos are of low quality, especially at a high bit rate, which can not obtain high human visual experience.

In the second category, solutions try to use a scalable bit stream to support human and machine vision simultaneously. Xia et al. [4] proposed to connect signal-level and task-level compact descriptors in a scalable manner. Only part of the scalable bit stream needs to be transmitted and decoded depending on subsequent tasks. Jin et al. [5] extended the

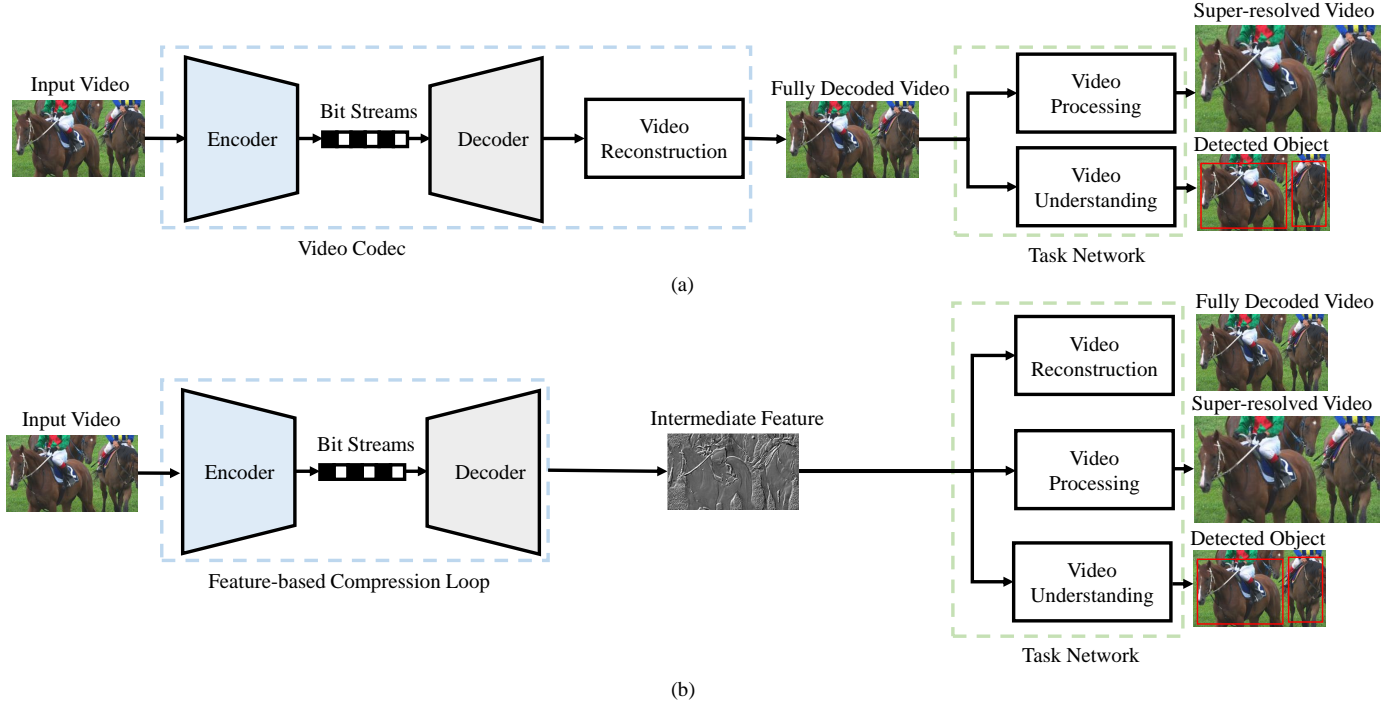


Fig. 1. (a) Overview of the *Reconstructing First, Processing Second* and *Reconstructing First, Analysis Second* paradigm. The encoder compresses input video into bit streams and the decoder decompresses the bit streams to a fully decoded video in the pixel domain. Then, video processing and video analysis algorithms are performed on the fully decoded video. (b) Overview of our proposed learned versatile video compression (LVVC) framework. The framework is comprised of a feature-based compression loop and a task network. The feature-based compression loop is used to encode the input video into bit streams and decode them to intermediate features. Obtaining the intermediate features, the task network allows users to choose to perform video reconstruction, video processing, such as video super-resolution, and video analysis, such as video object detection.

scalable bit stream to a semantically structured bit stream. Apart from the intermediate layer features of task networks, they also organized the output of task networks, such as bounding boxes of objects, into the bit stream. The design of their encoder depends on specific tasks. It is difficult to apply them to diverse or even unseen vision tasks without adjusting the encoder.

In the third category, solutions compress the videos using video codecs and then fully decode the bit stream into pixels for human and machine vision tasks. The anchor of a relative standard-video coding for machine [16]—developed by MPEG adopts this pattern. This kind of solution can achieve high compression efficiency for video reconstruction. However, it is inefficient for them to decode the bit stream into pixels before performing machine vision algorithms. Much computational burden is consumed for decoding the pixel-domain videos and the speed of vision tasks is decreased.

As far as we know, in the existing literature, there is no video codec that simultaneously meets the three requirements: 1) achieve high compression efficiency for video reconstruction and effective performance for human and machine vision tasks; 2) enable directly performing machine vision algorithms without decoding the bit stream into pixels; 3) be independent of the subsequent machine vision tasks.

2.2 Learned Video Coding

Existing learned video compression can be roughly categorized into four classes. In the first class, schemes [7], [9],

[17] follow a residual coding pattern. Motion-compensated prediction is first performed in the pixel domain or feature domain. Then the residue from the prediction is compressed by an autoencoder. In the second class, schemes [18], [19] apply the existing image codecs to video compression. Each frame is compressed into a compact representation by an image codec. Temporal entropy models are then built to explore the temporal correlations between each compact representation. In the third class, schemes [20], [21] use the 3D convolution-based autoencoder to compress multiple video frames directly. The schemes in these three classes may have the potential to apply to video processing and analysis without the need to obtain fully decoded videos in the pixel domain. Nevertheless, their compression efficiency is inferior to that of traditional video codecs [22], [23], [24].

To further increase the compression ratio of learned video codecs, schemes in the fourth class used a conditional coding paradigm to replace the residue coding in the first class. Li et al. [10] proposed the first conditional coding-based learned video codec. They learn temporal contexts from the previously decoded frame and then make the codec explore the temporal correlation automatically from the temporal contexts. Hoet al. [13] extended conditional coding to motion compression and Shi et al. [12] further used it for I frame coding. The conditional coding paradigm has made the learned video codecs catch up with or even surpassed traditional video codecs. However, learning temporal contexts from the previously decoded frame makes it infeasible to directly perform machine vision algorithms without fully decoding the bit stream into pixels. Although

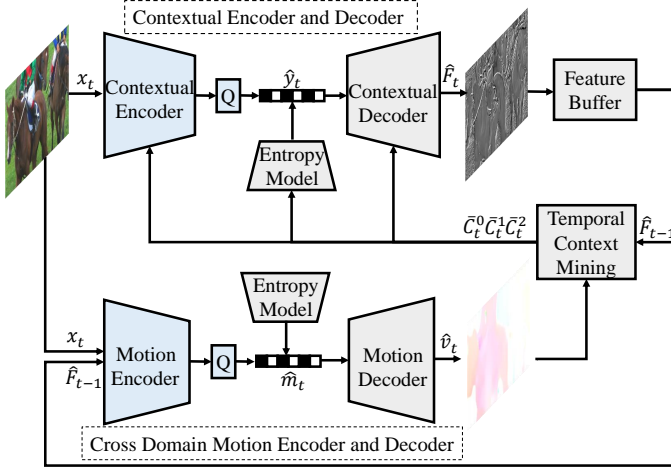


Fig. 2. Architecture of our proposed feature-based compression loop. The contextual encoder and decoder are proposed to compress the input frame x_t and decode it to an intermediate feature \hat{F}_t . The feature \hat{F}_t is regarded as a reference to help compress the next frame x_{t+1} . The feature-based temporal context mining module is used to learn multi-scale temporal contexts from previous intermediate feature \hat{F}_{t-1} . The temporal contexts $\bar{C}_t^0, \bar{C}_t^1, \bar{C}_t^2$ are used to improve the compression efficiency of the contextual encoder and decoder. The cross-domain motion encoder and decoder are proposed to compress and reconstruct the motion vector (MV) \hat{v}_t from the input frame x_t and previous intermediate feature \hat{F}_{t-1} . “Q” refers to the quantization operation.

Sheng et al. [11] proposed to learn temporal contexts from a propagated feature of the previous frame, the feature is very close to the fully reconstructed frame. When oriented to human-machine vision tasks, their decoder is still closely coupled with the full video reconstruction and only the computational cost of the last convolutional layer can be saved.

3 FRAMEWORK OVERVIEW

We illustrate an overview of our proposed learned versatile video compression framework in Fig. 1. The framework is comprised of a feature-based compression loop and a task network. The feature-based compression loop is used to compress videos into bit streams and reconstruct them to intermediate features. The task network allows users to perform multiple tasks directly from the intermediate feature, such as video reconstruction, video processing, and video analysis.

3.1 Feature-based Compression Loop

The architecture of the feature-based compression loop is shown in Fig. 2. It mainly includes a contextual encoder-decoder, a feature-based temporal context mining module, a cross-domain motion encoder-decoder, quantization, and entropy models.

Contextual Encoder and Decoder. The contextual encoder transforms an input frame x_t into a compact representation \hat{y}_t . The contextual decoder inversely transforms the compact representation to an intermediate feature \hat{F}_t . The feature \hat{F}_t is regarded as a reference feature in the feature-based compression loop to help compress the next frame x_{t+1} . Following the condition coding paradigm [11], we re-fill the multi-scale temporal contexts $\bar{C}_t^0, \bar{C}_t^1, \bar{C}_t^2$ learned

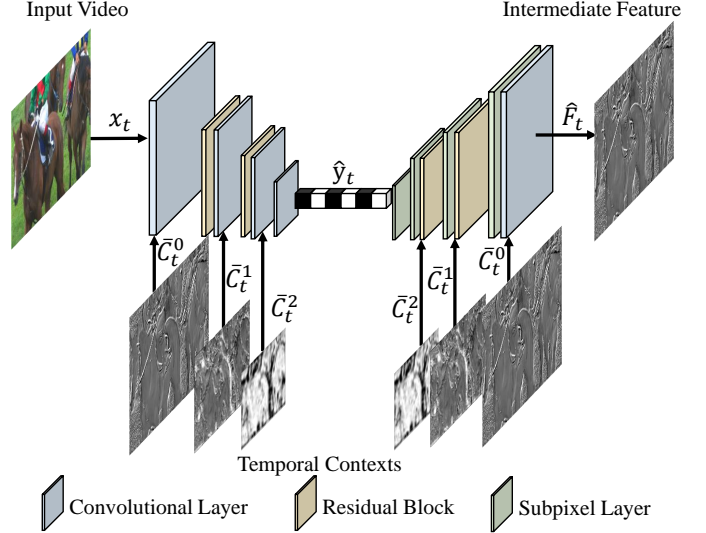


Fig. 3. Architecture for the contextual encoder-decoder. An autoencoder with a hyper-prior structure is adopted by the contextual encoder and decoder. Following a conditional coding paradigm, the multi-scale temporal contexts $\bar{C}_t^0, \bar{C}_t^1, \bar{C}_t^2$ learned by the temporal context mining module [11] are regarded as conditions and re-filled into the encoder and decoder.

by the feature-based temporal context mining module into the contextual encoder and decoder to explore the temporal correlation.

Feature-based Temporal Context Mining. One of the major reasons for the success of conditional coding is that it takes advantage of the temporal contexts. Previous conditional coding-based schemes learn temporal contexts from the previously decoded frame [10], [12], [13] or the feature of the last convolutional layer of the video reconstruction network [11], [14], which makes the decoding highly coupled with video reconstruction. In this work, we learn temporal contexts from the previous intermediate feature \hat{F}_{t-1} before being fed into the video reconstruction network to make the decoding decouple with reconstructed videos in the pixel domain. To make the temporal contexts contain richer temporal information, we follow the existing work [11] to learn multi-scale temporal contexts. The learned multi-scale temporal contexts $\bar{C}_t^0, \bar{C}_t^1, \bar{C}_t^2$ are re-filled into the contextual encoder-decoder and entropy modeling to explore temporal correlation.

Cross-Domain Motion Encoder and Decoder. Pre-trained optical flow networks [25], [26] are commonly used to estimate the motion vectors in the existing motion estimation and compensation-based learned video compression schemes. These schemes require the encoder to obtain the fully decoded videos in the pixel domain. Although some feature-based learned video codecs [9] used deformable convolutions to perform motion estimation in the feature domain, they also need to obtain the fully decoded videos first and then convert them to the feature domain. In this work, we propose a cross-domain motion encoder and decoder. It removes the separate motion estimation module and combines the motion estimation and compression together. The motion encoder directly compresses the previous intermediate feature \hat{F}_{t-1} and the current frame x_t into the compact representation \hat{m}_t and the motion decoder

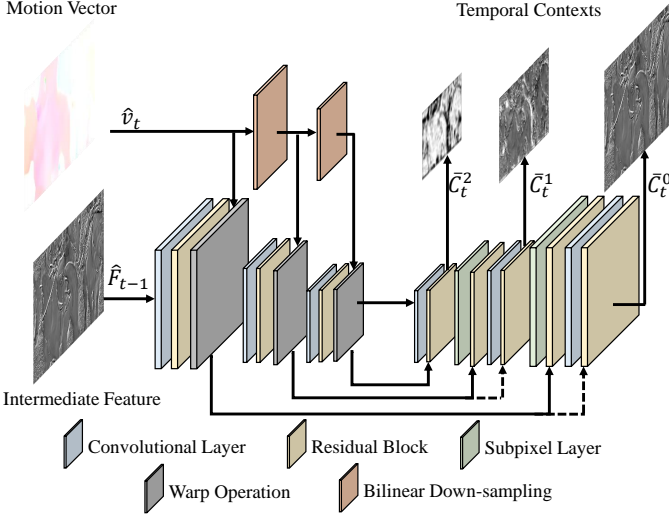


Fig. 4. Architecture for the feature-based temporal context mining module. Different from [11], the module learns multi-scale temporal contexts $\bar{C}_t^0, \bar{C}_t^1, \bar{C}_t^2$ from the previous intermediate feature \hat{F}_{t-1} before being fed into the video reconstruction network, which makes the decoding decouple with pixel-domain video reconstruction. The dotted lines refer to the addition operation.

produces the reconstructed motion vector \hat{v}_t . This scheme makes the encoder of the feature-based compression loop decouple with fully reconstructed videos in the pixel domain and greatly reduces the computational complexity for full video reconstruction and separate motion estimation modules.

Quantization and Entropy Modeling. Towards quantization, we add the uniform noise [27] to replace the quantization at the training stage and perform the exact rounding operation at the testing stage. Towards entropy modeling, we use the factorized entropy model [27] for hyper-prior and the Laplace distribution [28] to model the contextual and motion compact representations \hat{y}_t and \hat{m}_t . When estimating the mean and scale of the Laplace distribution of \hat{y}_t , we generate a temporal prior [11] from the multi-scale temporal contexts $\bar{C}_t^0, \bar{C}_t^1, \bar{C}_t^2$ to explore the temporal information. We do not apply the auto-regressive entropy model for parallel decoding.

3.2 Task Networks

Obtaining the intermediate feature \hat{F}_t generated by the contextual decoder, users can perform various tasks depending on their requirements, such as video reconstruction, video processing for human vision, and video analysis.

Video Reconstruction. The most basic task is video reconstruction. Even for video analysis tasks, further human analysis is required when the computer recognizes abnormal actions or detects the target object. For human visualization, the intermediate feature \hat{F}_t can be fed into a video reconstruction network to generate the fully decoded frame \hat{x}_t in the pixel domain. Experimental results in Section 8.2 show that a video reconstruction network with higher complexity can achieve higher reconstruction quality. However, a complex video reconstruction network requires more time to generate the fully decoded frame, which is not conducive to real-time computation for downstream video

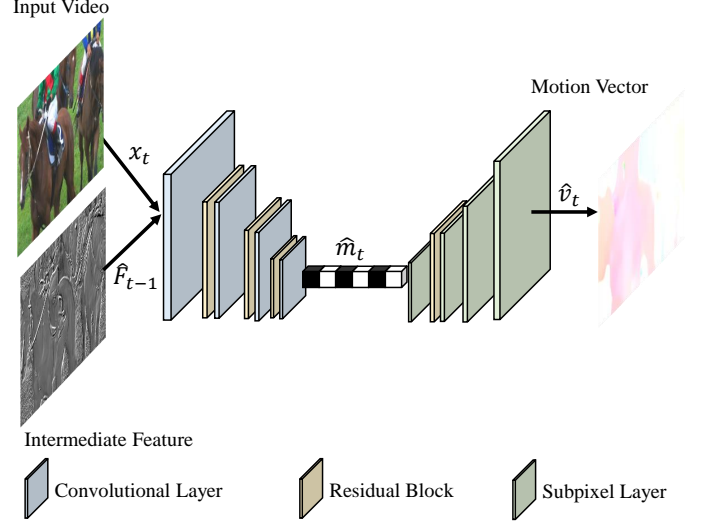


Fig. 5. Architecture for the cross-domain motion encoder and decoder. An autoencoder with a hyper-prior structure is adopted by the motion encoder and decoder. The motion encoder directly compresses the previous intermediate feature \hat{F}_{t-1} and the current frame x_t and the motion decoder produces the reconstructed motion vector \hat{v}_t .

processing and video analysis tasks. Therefore, we propose to directly perform downstream tasks from the intermediate feature \hat{F}_t rather than the fully decoded frame \hat{x}_t .

Video Processing. In our work, we directly process the intermediate feature \hat{F}_t without the need to obtain the fully decoded frame \hat{x}_t in the pixel domain. In addition, existing video processing schemes tend to use additional optical flow-based or deformable convolution-based temporal alignment modules to align the adjacent frames or features to take advantage of more temporal information. However, it is redundant for our framework. We can directly use the multi-scale temporal contexts $\bar{C}_t^0, \bar{C}_t^1, \bar{C}_t^2$, which have been aligned from the previous intermediate feature \hat{F}_{t-1} using the decoded motion vector \hat{v}_t . In our work, we take the most common video processing tasks, video denoising, and video super-resolution, as examples.

Video Analysis. Video analysis is another important downstream task of video compression in many real-world scenarios, such as video surveillance. In our work, we propose to directly analyze the intermediate feature \hat{F}_t without the need to obtain the fully decoded frame \hat{x}_t . We take video action recognition and video object detection as examples.

4 NETWORK ARCHITECTURES

4.1 Architectures for Feature-based Compression Loop

We mainly describe network architectures for our proposed contextual encoder-decoder, feature-based temporal context mining module, and cross-domain motion encoder-decoder.

Contextual Encoder and Decoder. The contextual encoder and decoder are based on an autoencoder with a hyper-prior structure. As illustrated in Fig. 3, the contextual encoder maps the input frame x_t to the compact representation with a $H/16 \times W/16$ resolution. In the mapping process, we concatenate the multi-scale temporal contexts $\bar{C}_t^0, \bar{C}_t^1, \bar{C}_t^2$ learned by the feature-based temporal context mining

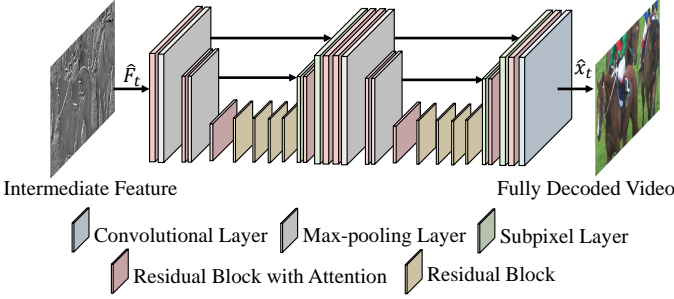


Fig. 6. Architecture for the video reconstruction network. The video reconstruction network is comprised of two cascaded U-shaped encoder-decoders for large receptive fields. The architecture of the residual block with attention can be found in [14].

module into the encoder. The compact representation is quantized before being sent to the arithmetic encoder which generates the bit stream. After receiving the bit stream, the arithmetic decoder decodes the bit stream to the compact representation. Symmetric with the contextual encoder, the contextual decoder reconstructs the compact representation to an intermediate feature \hat{F}_t with the conditions $\bar{C}_t^0, \bar{C}_t^1, \bar{C}_t^2$. The intermediate feature \hat{F}_t is used to help compress the next frame x_{t+1} or perform downstream tasks.

Feature-based Temporal Context Mining. As shown in Fig. 4, the feature-based temporal context mining module adopts a three-level hierarchical structure, which is the same as [11]. Differently, we feed the previous intermediate feature \hat{F}_{t-1} before being fed into the video reconstruction network to learn multi-scale temporal contexts $\bar{C}_t^0, \bar{C}_t^1, \bar{C}_t^2$. At each level of the hierarchical structure, we down-sample the decoded motion vector \hat{v}_t . Note that each down-sampled motion vector is divided by 2. Then, we use the down-sampled motion vectors to align the multi-scale features extracted from \hat{F}_{t-1} . Then the aligned features are up-sampled and fused together to generate the multi-scale temporal contexts $\bar{C}_t^0, \bar{C}_t^1, \bar{C}_t^2$.

Cross-Domain Motion Encoder and Decoder. The cross-domain motion encoder and decoder are also designed to be an autoencoder with a hyper-prior structure. As shown in Fig. 5, on the motion encoder side, the input frame x_t and the intermediate feature \hat{F}_{t-1} of the previous frame are concatenated together, and transformed into a compact representation with the resolution of $H/16 \times W/16$. Then the compact representation is quantized and encoded to a bit stream by the arithmetic encoder. On the motion decoder side, the received bit stream is decoded to the compact representation by the arithmetic decoder and then inversely transformed to the motion vector \hat{v}_t .

4.2 Network Architectures for Task Networks

Video Reconstruction. When users ask to display the video, we need to recover the intermediate feature \hat{F}_t to the fully decoded frame \hat{x}_t in the pixel domain. We use a video reconstruction network similar to [14]. As illustrated in Fig. 6, the video reconstruction network is comprised of two cascaded U-Nets [30]. Its large receptive field can improve the reconstruction capability effectively [14]. Specifically, the U-Nets consist of a contracting path and an expansive path. Residual blocks are used to perform convolutions on the input

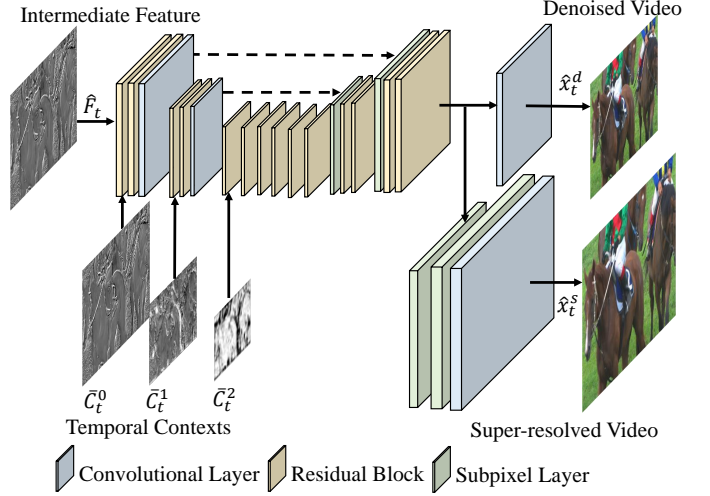


Fig. 7. Architecture for the video denoising network and video super-resolution network. The network is similar to the denoising block in [29]. To reduce the memory requirements, the merging of the features of the encoder with those of the decoder is done with an addition operation instead of a channel-wise concatenation.

reconstructed feature \hat{F}_t . To improve the representational power of the residual block and achieve dynamic channel-wise attention, a squeeze-and-excitation (SE) layer [31] is embedded into the residual block. In the contracting path, the residual blocks are connected by max-pooling layers to perform down-sampling. In the corresponding expansive path, subpixel layers are used to perform up-sampling. Different from [11], [14], we do not feed the temporal context \bar{C}_t^0 into the video reconstruction network to reduce the computational complexity.

Video Processing. When users ask to improve the quality of the decoded video for a better visual experience, we directly process the intermediate feature \hat{F}_t . We take video denoising and video super-resolution as examples.

For video denoising, we focus on the case of additive white Gaussian noise (AWGN), as done in existing video denoising work [29], [32]. We assume x_c is a clean image and n is the zero-mean white Gaussian noise of standard deviation δ , then the input frame x_t of the video codec is

$$x_t = x_c + n_t. \quad (1)$$

The input frame is compressed and decoded to the intermediate feature \hat{F}_t . To reduce the noise, we propose a simple denoising network with a U-Net structure which is similar to the denoising block in [29], as illustrated in Fig. 7. To reduce the memory requirements, the merging of the features in the contracting path with those in the corresponding expansive path is done with a pixel-wise addition operation instead of a channel-wise concatenation. To explore the temporal correlation of the previous frame, we feed aligned temporal contexts $\bar{C}_t^0, \bar{C}_t^1, \bar{C}_t^2$ obtained in the decoder side of feature-based compression loop into each one of the encoder layers of the denoising network.

For video super-resolution, we focus on $4\times$ video SR with Bicubic (BI) degradation. We assume x_t^L is a low-resolution frame. x_t^L is compressed and decompressed to the feature \hat{F}_t . We use the same network for video denoising

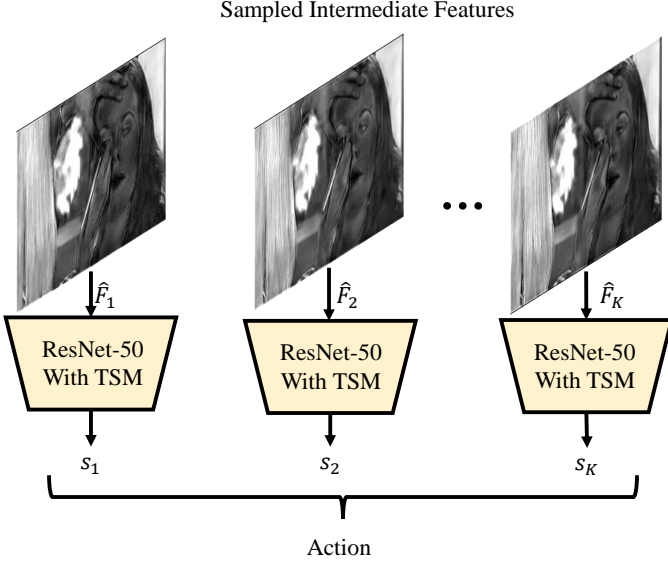


Fig. 8. Architecture for video action recognition. Given a compressed video, K decoded intermediate features $\hat{F}_1, \dots, \hat{F}_K$ are sampled. After sampling, ResNet-50 with TSM modules is used to process each of the sampled intermediate features individually. The output predicted class scores s_1, \dots, s_K are averaged to give the final prediction.

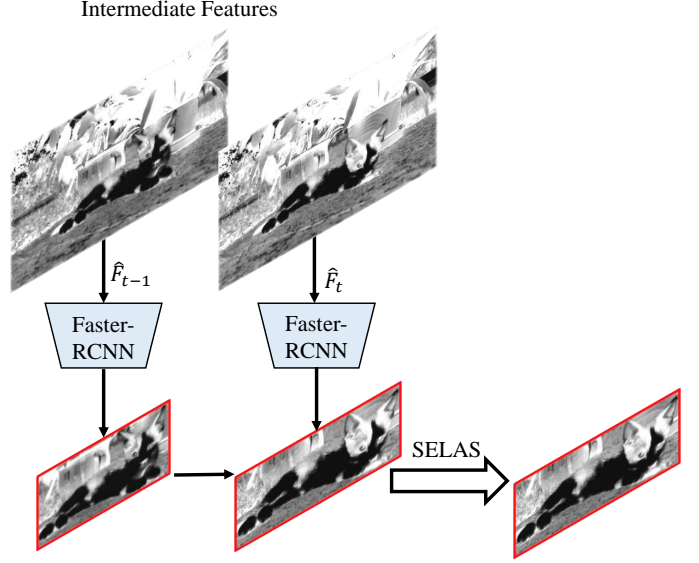


Fig. 9. Architecture for video object detection. Given a compressed video, we use ResNet-101 as the backbone network to process each of the decoded intermediate features. To aggregate the temporal information from the neighboring frame, we insert the sequence level semantics aggregation (SELSA) module after the fully-connected layer of Faster-RCNN. Different from the original SELAS model, which aggregates the temporal information of 14 neighboring frames, we only aggregate the temporal information of a single previous frame.

except that we add two subpixel layers before the last convolutional layer to achieve $4\times$ up-sampling.

Video Analysis. When users need to understand the video scenes, we can directly analyze the intermediate feature \hat{F}_t . We take video action recognition and video object detection as examples.

For video action recognition, we use the TSM [33] model as our baseline, as shown in Fig. 8. Specifically, given a compressed video, we first sample K intermediate features $\hat{F}_1, \dots, \hat{F}_K$. After sampling, we use 2D ResNet-50 [34] to process each of the features individually, and the predicted class scores are averaged to give the final prediction. To extract the high-level features of the intermediate features, the number of the input channel of ResNet-50 is modified to the channel number of the decoded features. Considering that the TSM model has a very large temporal receptive field to conduct highly complicated temporal modeling, we insert the TSM module into each residual block to enable temporal information fusion at no computation.

For video object detection, we apply the Faster-RCNN [35] model to detect objects. We use ResNet-101 as the backbone network to extract the high-level features of each intermediate feature \hat{F}_t . The number of the input channel of ResNet-101 is the same as the channel number of the decoded feature. To aggregate the features from the neighboring frame, we insert the sequence level semantics aggregation (SELSA) module [36] after the fully-connected layer of Faster-RCNN. However, different from the original SELAS model, which aggregates the temporal information of 14 neighboring frames, we only aggregate the temporal information of a single previous frame to achieve an online detection scheme, as illustrated in Fig. 9.

5 NETWORK OPTIMIZATION

5.1 Optimization for Feature-based Compression Loop

We adopt a step-by-step progressive training strategy to optimize the feature-based compression loop. Specifically, we first train the cross-domain motion encoder and decoder. We use the decoded motion vector \hat{v}_t to generate a predicted frame \hat{x}_t . Then we use the following rate-distortion cost to optimize the motion encoder-decoder,

$$L_m = \lambda d(x_t, \hat{x}_t) + R_m, \quad (2)$$

where $d(x_t, \hat{x}_t)$ denotes the distortion between the input frame x_t and the predicted frame \hat{x}_t . The distortion is measured by mean square error (MSE). R_m represents the bit rate used for encoding the quantized motion compact representation \hat{m}_t and the associated hyper-prior. Note that, the predicted frame is only used in the training stage for network optimization and there is no need to generate the predicted frame in the testing stage.

Then we fix the cross-domain motion encoder-decoder and train the contextual encoder-decoder. The target of contextual encoder-decoder is to compress a video frame into a bit stream with a smaller size and decompress the bit stream to an intermediate feature. However, we can not obtain the ground truth of the feature. Therefore, to generate an intermediate feature that is general enough for various tasks, we train the contextual encoder-decoder with the help of the video reconstruction network. Specifically, we convert the intermediate feature to a reconstructed frame with the video reconstruction network and then train the contextual encoder-decoder and the video reconstruction network jointly using the following loss function,

$$L_y = \lambda d(x_t, \hat{x}_t) + R_y, \quad (3)$$

where $d(x_t, \hat{x}_t)$ denotes the distortion between the input frame x_t and the reconstructed frame \hat{x}_t . The distortion is measured by MSE. R_y represents the bit rate used for encoding the quantized contextual compact representation \hat{y}_t and the associated hyper-prior.

Finally, we jointly optimize the rate-distortion cost of the whole feature-based compression loop,

$$L = \lambda d(x_t, \hat{x}_t) + R_m + R_y. \quad (4)$$

5.2 Optimization for Task Networks

Video Reconstruction. As described in Section 5.1, the video reconstruction network is part of the training process of the feature-based compression loop, users can directly use the trained video reconstruction network to generate fully decoded frame \hat{x}_t in the pixel domain. However, users are free to use other video reconstruction networks different from the one that helps train the feature-based compression loop. When training a new video reconstruction network, we fix the feature-based compression loop and use the MSE between the input frame x_t and the fully decoded frame \hat{x}_t to optimize the network.

Video Processing. Towards video processing, our framework targets to improve the quality of reconstructed frames while not harming the video compression performance. Therefore, we fix the feature-based compression loop and only optimize the video processing networks with their corresponding loss functions. We take video denoising and video super-resolution as examples. For video denoising, we use the MSE between the clean frame and the denoised frame to optimize the network. For video super-resolution, we use the MSE between the ground truth high-resolution frame and the super-resolved frame to optimize the network.

Video Analysis. Towards video analysis, we also fix the feature-based compression loop and only optimize the video analysis networks. We take video action recognition and video object detection as examples. For video action recognition, we follow the setting in [33] and use the standard categorical cross-entropy loss to optimize the network. For video object detection, we use the same multi-task loss in Faster R-CNN [35]. More details can be found in [33] and [35].

6 EXPERIMENTAL SETUP

To demonstrate the effectiveness of our proposed framework, we conduct extensive experiments on video reconstruction, video processing, and video analysis. Towards video reconstruction, we compare the compression efficiency of our framework with traditional video codecs and learned video codecs. Towards video processing and video analysis, we first use the same task network but different video codecs to explore the influence of video compression on corresponding tasks. Then, we use the same video codec but different task networks to verify the performance of different task networks against the compressed video.

6.1 Training Data

Video Reconstruction. We train the feature-based compression loop and video reconstruction network using the Vimeo-90k [37] dataset, which is a large-scale, high-quality video dataset. This dataset consists of 89,800 video clips and covers a large variety of scenes.

Video Denoising. We train the video denoising network using the DAVIS dataset [38]. DAVIS is a high-quality and high-resolution dataset under two resolutions, 480p and 1080p, which is widely used in video denoising. We use the 90 480p color videos for training.

Video Super-resolution. We train the video super-resolution network using the Vimeo-90k and REDS [39] datasets, respectively. REDS is a high-quality 720p video dataset proposed in the NTIRE19 Competition which contains 240 training videos.

Video Action Recognition. We train the video action recognition network on UCF101 dataset [40]. The UCF101 dataset contains 13,320 video clips that are divided into 101 action classes. The first split of the official training protocol [41] is adopted for training.

Video Object Detection. We train the video object detection network with a mixture of ImageNet VID and DET datasets [42] with the split provided in FGFA [43].

6.2 Testing Data

Video Reconstruction. We use three datasets HEVC [22], UVG [44], and MCL-JCV [45] to evaluate the reconstruction performance of our framework. HEVC dataset contains 16 commonly-used videos with different resolutions, including Class B, C, D, and E. Following the setting in [11], we add an additional HEVC Class RGB defined in the common test conditions for HEVC range extensions [46], which contains 6 1080p videos in RGB444 format. UVG and MCL-JCV datasets are also widely used. The UVG dataset has 7 1080p video sequences and the MCL-JCV dataset has 30 1080p video sequences.

Video Denoising. We use the DAVIS-test and Set8 dataset to benchmark our video denoising network. The DAVIS-test dataset contains 30 480p color sequences. The Set8 dataset is composed of 4 color sequences from the *Derf's Test Media collection* and 4 color sequences captured with a GoPro camera. Following the setting in [29], the sequences of the Set8 dataset are downsampled to a resolution of 960×540 .

Video Super-resolution. Following the setting in [47], when the video super-resolution network is trained on the Vimeo-90K dataset, we use Vid4 dataset [48] for evaluation. The Vid4 dataset consists of 4 color video sequences with different resolutions. When the network is trained on the REDS dataset, we use the REDS4 test dataset to evaluate the performance. REDS4 has 4 representative 720p videos selected from REDS with diverse scenes and motions.

Video Action Recognition. We evaluate our video action recognition network on UCF101 dataset [40]. Corresponding to the training set, the first split of the official testing protocol [41] is adopted for evaluation.

Video Object Detection. Following the existing work [36], [43], we evaluate our video object detection network on the ImageNet VID validation set, which contains 555 videos.

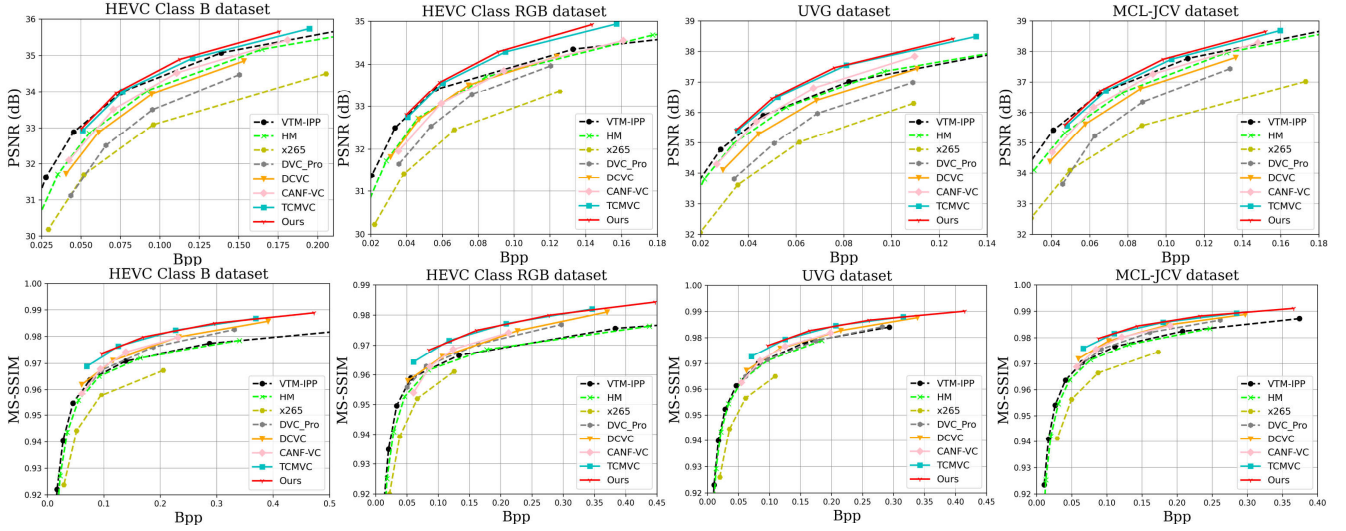


Fig. 10. Rate-distortion curves on the HEVC Class B, HEVC Class RGB, UVG, and MCL-JCV datasets. Intra period is set to 12.

TABLE 1
BD-rate for PSNR (intra period 12). The anchor is VTM-IPP.

	VTM-IPP	HM	x265	DVC_Pro	DCVC	CANF-VC	TCMVC	Ours
HEVC Class B	0.0	20.1	89.1	67.3	32.5	15.6	-1.0	-5.2
HEVC Class C	0.0	13.3	49.5	70.5	44.8	22.2	15.7	7.3
HEVC Class D	0.0	11.6	44.2	47.2	25.2	8.2	-3.4	-7.7
HEVC Class E	0.0	22.4	79.5	124.2	66.8	26.7	7.8	1.9
HEVC Class RGB	0.0	13.2	94.5	50.8	22.9	22.9	-13.7	-17.9
MCL-JCV	0.0	15.3	99.2	63.0	28.1	12.5	-1.6	-5.3
UVG	0.0	8.3	97.4	54.8	21.0	-1.6	-20.4	-22.3

TABLE 2
BD-rate for MS-SSIM (intra period 12). The anchor is VTM-IPP.

	VTM-IPP	HM	x265	DVC_Pro	DCVC	CANF-VC	TCMVC	Ours
HEVC Class B	0.0	14.9	72.3	-12.9	-25.2	-15.5	-49.5	-53.6
HEVC Class C	0.0	13.5	53.4	-11.8	-26.2	-21.3	-46.8	-50.2
HEVC Class D	0.0	10.6	46.0	-30.8	-40.1	-31.8	-56.5	-58.4
HEVC Class E	0.0	17.0	60.8	17.3	-8.0	1.3	-50.1	-56.4
HEVC Class RGB	0.0	14.7	68.6	-13.1	-24.3	-4.3	-50.9	-53.6
MCL-JCV	0.0	14.1	75.4	-12.0	-26.8	-17.6	-40.6	-44.7
UVG	0.0	10.2	73.5	4.7	-9.2	-3.4	-29.1	-32.6

6.3 Implementation Details

Video Reconstruction. Towards video reconstruction, we crop the training video frames to 256×256 patches. Following previous work [10], [11], [13], four models with different λ values ($\lambda = 256, 512, 1024, 2048$) are trained for different coding rates. We use AdamW [49] optimizer and set the batch size to 4. When using MS-SSIM [50] for performance evaluation, we fine-tune the model by using 1-MS-SSIM as the distortion. Meanwhile, each λ value is divided by 50.

Video Denoising. Towards video denoising, 256×256 training patches are also used. For each λ value, we train two models for different white Gaussian noise (standard deviation $\delta=20$ and 40). The optimizer and batch size settings are the same as video reconstruction.

Video Super-resolution. Towards video super-resolution, we crop the video frames to patches of size 64×64 . The corresponding 256×256 high-resolution patches are regarded as the ground truth. We train a single

model for each individual λ value. The optimizer and batch size settings are the same as those of video reconstruction and denoising.

Video Action Recognition. We use MMac-tion2 [51] to implement our video action recognition network. The default configuration file for TSM *tsm_k400_pretrained_r50_1x1x8_25e_ucf101_rgb.py* is used for our network.

Video Object Detection. We use MMtracking [52] to implement our video object detection network. The configuration file for SELSA *selsa_faster_rcnn_r101_dc5_1x_imagenetvid.py* is used to train and evaluate our network. Different from the original SELSA model, which aggregates the temporal information of 14 neighboring frames, we only aggregate the temporal information of a single previous frame.

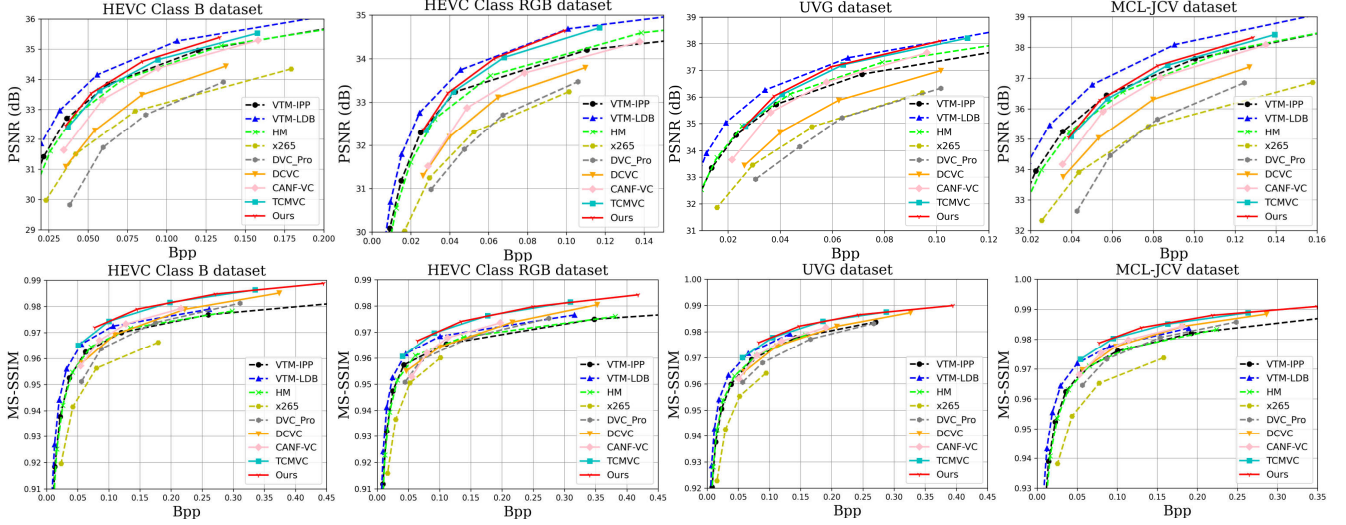


Fig. 11. Rate-distortion curves on the HEVC Class B, HEVC Class RGB, UVG, and MCL-JCV datasets. Intra period is set to 32.

TABLE 3
BD-rate for PSNR (intra period 32). The anchor is VTM-IPP.

	VTM-IPP	VTM-LDB	HM	x265	DVC_Pro	DCVC	CANF-VC	TCMVC	Ours
HEVC Class B	0.0	-22.2	9.0	94.8	149.2	70.2	21.7	0.3	-6.1
HEVC Class C	0.0	-25.7	4.0	51.6	144.7	87.5	25.0	16.6	6.5
HEVC Class D	0.0	-23.7	3.6	47.7	104.9	58.0	8.9	-5.7	-10.6
HEVC Class E	0.0	-24.0	11.1	91.5	352.1	202.5	67.4	24.8	19.0
HEVC Class RGB	0.0	-28.6	1.7	101.0	121.5	65.0	37.0	-14.2	-18.8
MCL-JCV	0.0	-25.5	7.7	103.6	119.8	55.9	20.7	2.7	-1.3
UVG	0.0	-31.9	-4.4	104.4	128.8	58.1	6.4	-18.3	-20.7

TABLE 4
BD-rate for MS-SSIM (intra period 32). The anchor is VTM-IPP.

	VTM-IPP	VTM-LDB	HM	x265	DVC_Pro	DCVC	CANF-VC	TCMVC	Ours
HEVC Class B	0.0	-23.5	4.4	78.1	15.8	-10.9	-11.2	-47.3	-54.4
HEVC Class C	0.0	-25.1	3.5	56.0	15.4	-12.9	-18.2	-46.5	-52.2
HEVC Class D	0.0	-23.8	3.1	49.6	-12.9	-30.4	-31.2	-57.4	-60.9
HEVC Class E	0.0	-23.1	8.5	71.8	112.6	52.2	40.4	-41.2	-51.1
HEVC Class RGB	0.0	-24.3	4.1	75.1	15.7	-9.3	40.8	-50.3	-56.0
MCL-JCV	0.0	-25.5	6.2	81.4	7.0	-17.9	-16.0	-38.2	-44.7
UVG	0.0	-28.4	-2.2	79.6	28.4	3.9	-0.1	-27.4	-32.7

TABLE 5
Average encoding/decoding time for a 1080p frame on the same NVIDIA 1080Ti platform (in seconds).

Schemes	Enc Time	Dec Time
DVC_Pro	8.97	56.29
DCVC	9.62	57.41
CANF-VC	2.23	1.11
TCMVC	1.87	1.39
Ours	1.49	1.41

7 EXPERIMENTAL RESULTS

7.1 Results for Video Reconstruction

To verify the compression performance of our framework, we compare it with the traditional video codecs of H.265 [22], and H.266 [24]. Specifically, for H.265, we compare with its industrial software x265 under *veryslow* preset and official reference software HM under *en-*

coder_lowdelay_main_rext configuration. For H.266, we compare with its official reference software VTM. Following the setting in [11], we use the VTM-LDB (*encoder_lowdelay_vtm*) and VTM-IPP (one reference frame and flat QP) configurations. Furthermore, previous state-of-the-art learned video compression schemes are also included for comparison, including DVC_Pro [7], DCVC [10], CANF-VC [13], TCMVC [11]. For CANF-VC and TCMVC, we use their models with error propagation training [11]. For all the learned video codecs, we use the unified *cheng2020anchor* model without the auto-regressive entropy model as the I-frame codec. We set the intra period to 12 and 32 and encode 96 frames for each video in all testing datasets.

We first list the BD-rate results for intra period 12 in Table 1 and Table 2. When calculating the BD-rate, we regard VTM-IPP as the anchor. VTM-LDB is not used for comparison when the intra period is 12 since the GOP size of *encoder_lowdelay_vtm* configuration is 8 and it does

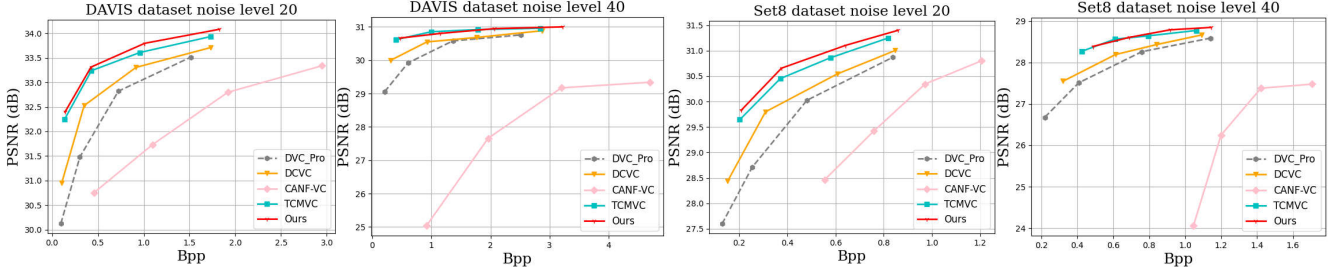


Fig. 12. Rate-performance (PSNR between denoised videos and clean videos) curves on the DAVIS dataset and Set8 dataset. The fully decoded videos in the pixel domain are denoised by FastDVDnet. The standard deviation δ values of the white Gaussian noise of the input noisy videos are set to 20 and 40.

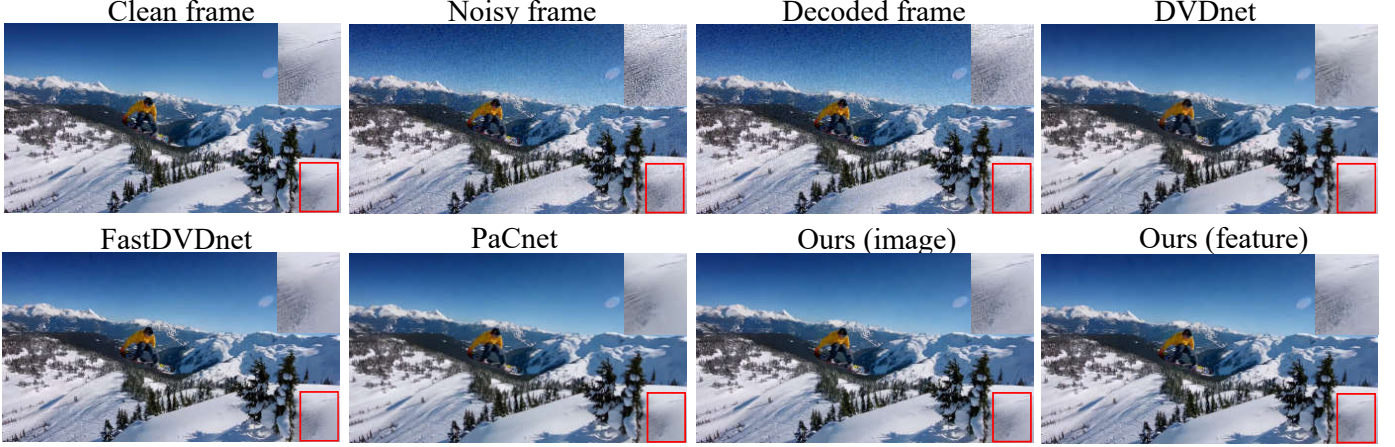


Fig. 13. Comparison results of the “snowboarding” sequence in Set8 dataset when $\delta = 40$.

TABLE 6
Video denoising results for PNSR (dB) on DAVIS dataset.

Methods	Params (M)	Runtime (s/frame)	$\delta=20$				$\delta=40$			
			$\lambda=256$	$\lambda=512$	$\lambda=1024$	$\lambda=2048$	$\lambda=256$	$\lambda=512$	$\lambda=1024$	$\lambda=2048$
Ours (feature)	7.2+2.5	0.016+0.009	32.46	33.46	34.09	34.42	30.95	31.26	31.61	31.77
Ours (image)	10.7+2.4	0.028+0.008	32.81	33.80	34.33	34.68	31.16	31.62	31.87	32.02
DVDnet	10.7+1.3	0.028+0.238	31.35	31.92	32.23	32.39	29.24	29.42	29.55	29.61
FastDVDnet	10.7+2.5	0.028+0.077	32.39	33.31	33.79	34.08	30.66	30.80	30.95	31.00
PaCnet	10.7+2.9	0.028+23.112	32.34	33.17	33.60	33.91	30.85	31.16	31.37	31.48

TABLE 7
Video denoising results for PNSR (dB) on Set8 dataset.

Methods	Params (M)	Runtime (s/frame)	$\delta=20$				$\delta=40$			
			$\lambda=256$	$\lambda=512$	$\lambda=1024$	$\lambda=2048$	$\lambda=256$	$\lambda=512$	$\lambda=1024$	$\lambda=2048$
Ours (feature)	7.2+2.5	0.016+0.011	29.83	30.73	31.34	31.66	28.63	28.93	29.27	29.43
Ours (image)	10.7+2.4	0.028+0.009	30.14	31.07	31.59	31.96	28.81	29.22	29.50	29.64
DVDnet	10.7+1.3	0.028+0.328	29.03	29.67	30.01	30.23	27.24	27.49	27.66	27.72
FastDVDnet	10.7+2.5	0.028+0.093	29.83	30.66	31.10	31.40	28.39	28.61	28.79	28.85
PaCnet	10.7+2.9	0.028+25.245	29.66	30.42	30.82	31.13	28.21	28.49	28.70	28.80

not support intra period 12. Experimental results show that for intra period 12 and oriented to PSNR, our proposed framework outperforms HM on all the datasets and even achieves a higher compression performance than VTM-IPP on most datasets, especially for the UVG dataset (22.3%). When oriented to MS-SSIM, our framework can achieve more than 50% BD-rate reduction. We also list the BD-rate results when the intra period is set to 32 in Table 3 and Table 4. Experimental results show that for intra

period 32, the compression performance of most learned video codecs is greatly reduced while our framework still achieves a comparable compression performance compared with VTM-IPP. It should be noted that our framework is extendable and easy to be followed. More advanced coding tools can be easily integrated into our framework for higher compression performance, such as more powerful I-frame codec, transform, and entropy models [14].

We also list the average encoding and decoding time



Fig. 14. Comparison results of the “calendar” sequence in the Vid4 dataset.

TABLE 8
Video super-resolution results for PNSR (dB) on REDS4 datasets.

Methods	Params (M)	Runtime (s/frame)	REDS4			
	Dec+Task	Dec+Task	$\lambda=256$	$\lambda=512$	$\lambda=1024$	$\lambda=2048$
Ours (feature)	7.2+2.8	0.015+0.009	24.65	25.26	25.89	26.25
Ours (image)	10.7+2.7	0.027+0.009	24.67	25.32	25.89	26.29
TDAN	10.7+2.0	0.027+0.025	24.62	25.19	25.74	26.15
MuCAN	10.7+13.6	0.027+3.151	24.63	25.22	25.84	26.33
EDVR	10.7+20.6	0.027+1.925	24.62	25.21	25.97	26.16

TABLE 9
Video super-resolution results for PNSR (dB) on Vid4 datasets.

Methods	Params (M)	Runtime (s/frame)	Vid4			
	Dec+Task	Dec+Task	$\lambda=256$	$\lambda=512$	$\lambda=1024$	$\lambda=2048$
Ours (feature)	7.2+2.8	0.014+0.008	21.15	21.64	22.11	22.43
Ours (image)	10.7+2.7	0.025+0.008	21.15	21.62	22.11	22.37
TDAN	10.7+2.0	0.025+0.024	21.16	21.62	22.08	22.50
MuCAN	10.7+13.6	0.025+1.973	21.16	21.63	22.16	22.66
EDVR	10.7+20.6	0.025+0.943	21.15	21.62	22.13	22.63

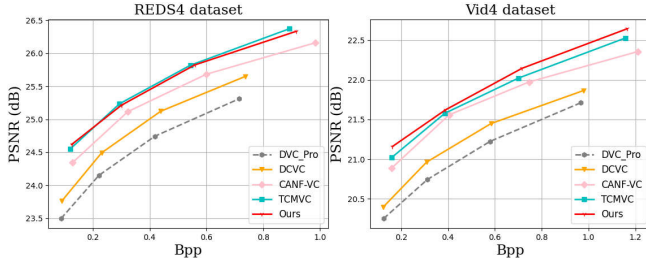


Fig. 15. Rate-performance (PSNR between the output super-resolved videos and the ground truth high-resolution videos) curves on the REDS4 and Vid4 datasets. The fully decoded low-resolution videos are super-resolved by EDVR.

for one 1080p frame of different learned video codecs in Table 5. The comparison results show that the encoding time of our proposed framework is the shortest since its encoder removes the separate motion estimation network and does not need to obtain the full reconstructed videos in the pixel domain. The decoding time of our framework is a little more than CANF-VC and TCMVC since it uses a more complex video reconstruction network on the decoder side for higher compression efficiency. However, when oriented to video

processing and analysis, the video reconstruction network can be removed.

7.2 Results for Video Denoising

In this experiment, we first use the same video denoising network but different learned video codecs to explore the influence of video compression on video denoising. We then use the same video codec but different video denoising networks to verify the performance of different video denoising networks against the compressed video.

To explore the influence of video compression on video denoising, we use DVC_Pro, DCVC, CANF-VC, TCMVC, and our proposed video codec to compress noisy videos. The standard deviation δ values of the white Gaussian noise of the input noisy videos are set to 20 and 40. Then we fully decode the videos into pixel domain and feed them into FastDVDnet [29] to perform denoising. The rate-performance curves on DAVIS and Set8 datasets are illustrated in Fig. 12. We use PSNR as the performance evaluation metric. The comparison results show that the videos decoded by our proposed learned codec can achieve the best denoising performance.

TABLE 10
Video action recognition results for top1-accuracy (%) on on the first testing split of the UCF101 dataset.

Methods	Params (M)	Runtime (s/video)	Backbone	$\lambda=256$	$\lambda=512$	$\lambda=1024$	$\lambda=2048$
	Dec+Task	Dec+Task					
Ours (feature)	7.2+23.9	2.76+0.34	ResNet-50	91.1	91.3	92.2	92.4
Ours (image)	10.7+23.7	4.60+0.33	ResNet-50	90.1	91.6	92.9	93.4
I3D	10.7+28.0	4.60+0.79	ResNet-50	84.5	85.5	85.8	86.1
Slowonly	10.7+31.8	4.60+1.05	ResNet-50	89.6	90.9	91.8	92.2
C3D	10.7+78.4	4.60+0.91	c3d	80.5	81.3	81.7	82.3

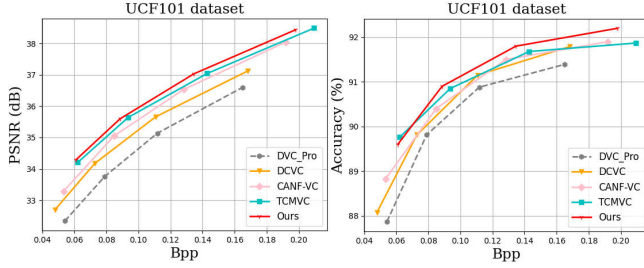


Fig. 16. Rate-distortion curves and rate-performance (video action recognition top1-accuracy) curves on the first testing split of the UCF101 dataset. The fully decoded low-resolution videos in the pixel domain are recognized by Slowonly.

To verify the performance of different video denoising networks against the compressed video, we first use our proposed codec to generate the intermediate feature \hat{F}_t or fully decoded video in the pixel domain \hat{x}_t and then feed them into different video denoising networks. Specifically, for our proposed video denoising network illustrated in Fig. 7, we directly feed the intermediate feature \hat{F}_t into it to perform denoising. We refer to it as *Ours (feature)*. To evaluate the video denoising performance of *Ours (feature)*, we design a variant network and refer to it as *Ours (image)*. The variant network has the same architecture as *Ours (feature)* except that the number of input channels of the first convolutional layer is set to 3. We also compare with some baseline video denoising networks, including DVDNet [32], FastDVDnet [29], and PaCnet [53]. For *Ours (image)* and all the baselines, we feed the fully decoded videos in the pixel domain into them and then perform denoising. Table 6 and 7 present the video denoising results under different standard deviations δ and different compression ratios λ on the DAVIS dataset and Set8 dataset, respectively. We also illustrate the subjective results of the “snowboarding” sequence in the Set8 dataset when $\delta = 40$ in Fig. 13. Comparing *Ours (image)* and *Ours (feature)*, *Ours (image)* achieves a slightly better denoising result than *Ours (feature)*. This may be owing to that its video reconstruction network and the video denoising network form a two-stage denoiser [54]. However, *Ours (feature)* scheme can save much complexity burden to obtain decoded videos in the pixel domain. Take the DAVIS dataset as an example, the number of parameters of the decoder of *Ours (image)* is 3.5M (10.7M-7.2M) more than that of the decoder of *Ours (feature)*. The runtime (0.028s-0.016s) of converting the intermediate feature to the pixel domain is even more than the video denoising time. Therefore, directly processing the intermediate feature is more suitable for real-time applications.

7.3 Results for Video Super-resolution

Similar to video denoising, in this experiment, we first use the same video super-resolution network but different learned video codecs to explore the influence of video compression on video super-resolution. We then use the same video codec but different video super-resolution networks to verify the performance of different video super-resolution networks against the compressed video.

To explore the influence of video compression on video super-resolution, we first compress low-resolution videos using DVC_Pro, DCVC, CANF-VC, TCMVC, and our proposed video codec. Then we use EDVR [47] to perform video super-resolution on the fully decoded videos in the pixel domain. The rate-performance curves on REDS4 and Vid4 datasets are presented in Fig. 15. PSNR is used as the performance evaluation metric. The comparison results show that the videos decoded by our proposed learned codec can achieve a better super-resolution performance on the Vid4 dataset and a similar performance compared with TCMVC on the REDS4 dataset.

To verify the performance of different video super-resolution networks against the compressed video, we use our proposed codec to generate intermediate features or pixel-domain decoded videos and then feed them into different video super-resolution networks. Specifically, for our proposed video super-resolution network illustrated in Fig. 7, we directly feed the intermediate features into it. We refer to it as *Ours (feature)*. To verify the effectiveness of *Ours (feature)*, we design a variant network that has the same architecture as *Ours (feature)* except that the number of input channels of the first convolutional layer is changed to 3. We refer to the variant network as *Ours (image)*. We also compare with some baseline video super-resolution networks, including TDAN [55], MuCan [56], and EDVR [47]. For *Ours (image)* and all the baselines, video super-resolution is performed on fully decoded frame \hat{x}_t in the pixel domain. We list the video super-resolution results on the REDS4 and Vid4 datasets in Table 9. We also illustrate the subjective results of the “calendar” sequence in the Vid4 dataset in Fig. 14 for comparison. Comparing *Ours (image)* and *Ours (feature)*, performing super-resolution on the pixel-domain decoded frames or the intermediate features obtain similar performance. However, *Ours (feature)* can save the complexity of converting the intermediate features to the fully decoded frames in the pixel domain. Taking the REDS4 dataset as an example, the runtime (0.027s-0.015s) used to convert the intermediate feature to the fully decoded frame is even more than that used for super-resolution.

TABLE 11
Video object detection results for box AP@50 (%) on ImageNet VID validation dataset.

Methods	Params (M)	Runtime (s/frame)	Reference	Backbone	$\lambda=256$	$\lambda=512$	$\lambda=1024$	$\lambda=2048$
	Dec+Task	Dec+Task						
Ours (feature)	7.2+85.8	0.016+0.094	1	ResNet-101	69.7	70.3	71.3	72.2
Ours (image)	10.7+85.6	0.029+0.093	1	ResNet-101	70.8	71.1	71.9	73.4
DFF	10.7+114.5	0.029+0.060	1	ResNet-101	67.9	69.7	70.7	71.3
FGFA	10.7+116.8	0.029+0.556	30	ResNet-101	72.7	74.3	75.5	76.1
SELAS	10.7+85.6	0.029+0.454	14	ResNet-101	79.3	80.1	80.7	81.1

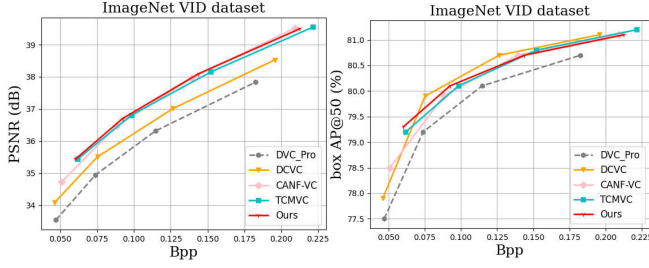


Fig. 17. Rate-distortion and rate-performance (video object detection box AP@50) curves on ImageNet VID validation dataset. The fully decoded videos in the pixel domain are recognized by SELAS.

7.4 Results for Video Action Recognition

Besides the human vision tasks, we also need to explore the influence of video compression on machine vision tasks. In this experiment, we first use the same video action recognition network but different learned video codecs to explore the influence of video compression on video action recognition. We then use the same video codec but different video action recognition networks to verify the performance of different video action recognition networks against the compressed video.

To explore the influence of video compression on video action recognition, we use DVC_Pro, DCVC, CANF-VC, TCMVC, and our proposed video codec to compress the videos in the first testing split of the UCF101 dataset. Then we feed their fully decoded videos in the pixel domain into Slowonly [57] to perform video action recognition. The rate-distortion curves and rate-performance curves are illustrated in Fig. 16. We use recognition top1-accuracy(%) as the performance evaluation metric. The comparison results show that the quality of the reconstructed videos is closely related to the accuracy of the video action recognition. The higher the quality of the reconstructed videos, the higher the accuracy of video action recognition. Our proposed video codec can achieve the best reconstruction performance and highest action recognition accuracy.

To verify the performance of different video action recognition networks against the compressed video, we first use our proposed codec to generate intermediate features or fully decoded videos in the pixel domain and then feed them into different video action recognition networks. Specifically, for our proposed video action recognition network *Ours (feature)*, we directly feed the intermediate features into it to perform video action recognition. To verify the effectiveness of *Ours (feature)*, we compare it with its variant network *Ours (image)* which recognizes from the fully decoded videos. *Ours (image)* has the same architecture

as *Ours (feature)* except that the number of input channels of the first convolutional layer is changed to 3. Actually, *Ours (image)* is the same as the original TSM model. We also compare *Ours (feature)* and *Ours (image)* with C3D [58], I3D [59], and Slowonly [57]. We list the top1-accuracy (%) results in Table 10. Comparing *Ours (feature)* and *Ours (image)*, their action recognition accuracy is similar, which shows that the TSM module is also effective for the intermediate feature. Most existing action recognition networks sample a part of frames from an entire video and only need to predict the sampled frames. Sampled frames are only available after the entire video is decoded. The experimental results show that decoding an entire video takes much more time than recognizing a video. Therefore, decreasing the video decoding time is necessary for action recognition. Comparing the runtime of *Ours (feature)* and *Ours (image)*, *Ours (feature)* can save much decoding time (4.60s-2.76s) used to convert the intermediate feature to the fully decoded frame.

7.5 Results for Video Object Detection

Similar to the above-mentioned experiments, we first use the same video object detection network but different learned video codecs to explore the influence of video compression on video object detection. Then, we use the same video codec but different video object detection networks to verify the performance of different video object detection networks against the compressed video.

To explore the influence of video compression on video object detection, we compress the videos of the ImageNet VID validation dataset using DVC_Pro, DCVC, CANF-VC, TCMVC, and our proposed video codec. Then we use SELAS to detect their pixel-domain decoded videos. The rate-distortion curves and rate-performance curves are presented in Fig. 17. We use the box AP50 as the performance evaluation metric. The experimental results show that, for video reconstruction, our proposed video codec achieves the highest performance on the ImageNet VID validation dataset. For video object detection, DCVC achieves better performance than our codec, especially at higher bit rates. This may be owing to that our codec uses more bits to keep more high-frequency texture details while keeping these details can not bring obvious performance improvement for object detection.

To verify the performance of different video object detection networks against the compressed video, we first use our proposed codec to generate intermediate features or fully decoded videos in the pixel domain and then feed them into different video object detection networks. Specifically, for our proposed video object detection network *Ours (feature)*,

TABLE 12

Effectiveness of the cross-domain motion encoder and decoder on HEVC dataset.

Methods	Params (M)		B	C	D	E	RGB
	Enc	Dec					
Ours	11.3	10.7	0.0	0.0	0.0	0.0	0.0
pixel-domain	15.7	10.7	-1.6	-1.0	-2.1	2.9	1.2

TABLE 13

Influence of the complexity of the video reconstruction network on video compression on HEVC dataset.

Methods	B	C	D	E	RGB
Ours	0.0	0.0	0.0	0.0	0.0
1 U-Net	0.9	1.0	0.2	2.1	1.5
2 residual blocks	3.1	2.2	1.2	5.7	3.7
1 residual blocks	3.0	3.3	2.1	6.5	4.7

we directly detect the intermediate feature. To evaluate the effectiveness of *Ours (feature)*, we design a variant network *Ours (image)* which performs object detection from the fully decoded videos in the pixel domain. *Ours (image)* has the same architecture as *Ours (feature)* except that the number of input channels of the first convolutional layer is changed to 3. We also compare our video object detection networks with DFF [60], FGFA [43], and SELAS [36]. Table 11 lists the video object detection results for box AP@50 on the ImageNet VID dataset. Compared with FGFA and SELAS, *Ours (image)* and *Ours (feature)* achieve much lower accuracy. This is because FGFA and SELAS aggregate the temporal information of 30 and 14 reference frames while our networks only use a single reference frame. Note that, as reported in [36], SELAS with a single reference frame achieves 73.62% box AP@50 on the uncompressed ImageNet VID validation dataset. Compared with DFF, which also uses one reference frame, we achieve higher performance but we do not need the additional optical flow estimation module. Comparing *Ours (image)* and *Ours (feature)*, *Ours (feature)* is slightly worse than *Ours (image)* but saves more computational complexity.

8 ABLATION STUDY AND ANALYSIS

8.1 Analysis of Cross-Domain Motion Encoder and Decoder

We build a variant model to verify the effectiveness of our proposed cross-domain motion encoder and decoder. Following previous work [10], [11], the variant model uses a pre-trained Spynet [25] to estimate the motion vector from the current input frame x_t and previously fully decoded frame \hat{x}_{t-1} . The estimated motion vector v_t is compressed and then decoded to \hat{v}_t using the same motion encoder-decoder with the same structure as Fig.5 except that the number of input channels is changed to 2. We list the BD-rate results on the HEVC datasets in Table 12. When calculating the BD-rate, we regard our framework (Ours) with cross-domain motion encoder-decoder as the anchor. From Table. 12, we find that the variant model (*pixel-domain*) can get a little better compression performance on a part of classes while it costs more parameters (4.4M) for Spynet

TABLE 14

Influence of the temporal contexts on video denoising for PNSR (dB) on DAVIS dataset when the standard deviation δ value of white Gaussian noise is set to 40.

Methods	$\delta=40$			
	$\lambda=256$	$\lambda=512$	$\lambda=1024$	$\lambda=2048$
Ours	30.95	31.26	31.61	31.77
Ours w/o contexts	30.85	31.11	31.46	31.58

TABLE 15

Influence of the temporal contexts on video super-resolution for PNSR (dB) on REDS dataset.

Methods	$\lambda=256$	$\lambda=512$	$\lambda=1024$	$\lambda=2048$
Ours	24.65	25.26	25.89	26.25
Ours w/o contexts	24.64	25.25	25.83	26.20

and pixel-domain video reconstruction in the encoder. The experimental results demonstrate that the effectiveness of using a pre-trained optical flow network to estimate motion vector is limited. Our proposed cross-domain motion encoder and decoder can not only maintain the efficiency of motion estimation and compression but also greatly reduce the complexity of encoding.

8.2 Influence of the Complexity of the Video Reconstruction Network

The complexity of the decoder affects the compression performance [14], [61]. To explore the influence of the complexity of the video reconstruction network in our proposed framework on the performance of video compression, we perform another experiment by replacing the video reconstruction network which is made up of two cascaded U-Nets with one U-Net, two residual blocks, and one residual block. The BD-rate comparison results on the HEVC datasets are shown in Table 13. The anchor is our framework (Ours) with the video reconstruction network consisting of two cascaded U-Nets. From this table, we can find that the compression performance increases a lot when the complexity of the video reconstruction network increases. This proves that when high-quality reconstructed videos are needed, a high-complexity video reconstruction network is needed to transform the intermediate feature \hat{F}_t to a fully decoded frame \hat{x}_t in the pixel domain. However, when oriented to video processing and video analysis tasks, the redundant video reconstruction network takes a large complexity burden. Therefore, directly processing and analyzing the intermediate feature \hat{F}_t can save much redundant computational complexity.

8.3 Influence of the Temporal Contexts on Video Processing

It is essential for video processing schemes to aggregate the features of neighboring frames. To achieve this target, temporal alignment modules, such as optical flow estimation networks or deformable convolutions are often used to generate the aligned temporal features. In our proposed framework, the aligned temporal features of the neighboring frame can be directly obtained in the decoder side

of the feature-based compression loop, i.e., the multi-scale temporal contexts \bar{C}_t^0 , \bar{C}_t^1 , \bar{C}_t^2 . Therefore, we directly feed \bar{C}_t^0 , \bar{C}_t^1 , \bar{C}_t^2 into video processing networks to utilize the temporal information. To explore the influence of the temporal contexts on video processing, we conduct a comparison experiment by removing the temporal contexts of the video denoising network and video super-resolution network. For video denoising, we conduct the experiment on the DAVIS dataset and set the standard deviation δ value of white Gaussian noise to 40. For video super-resolution, we report the results on the REDS4 dataset. The comparison results are listed in Table 14 and Table 15. The results show that the temporal contexts can effectively improve the video processing performance, which verifies the importance of aggregating the temporal information.

9 CONCLUSION

In this paper, we propose a versatile learned video compression framework for efficient human-machine vision. Different from the existing video coding schemes, where one compressed frame shall be reconstructed to pixels so as to be referenced for encoding/decoding the following frames, our framework has a feature-based compression loop, where one frame is encoded (resp. decoded) to intermediate features, and the intermediate features are referenced for encoding (resp. decoding) the following frames. The intermediate features may be used to reconstruct the videos in the pixel domain, or be fed into different task networks for various processing/analysis tasks directly. Extensive experimental results show that our proposed framework can achieve high compression efficiency and task performance simultaneously. Based on the proposed framework, we can plug any new coding tools into it for higher compression efficiency and can apply it to more human and machine vision tasks according to the user requirements.

REFERENCES

- [1] L.-Y. Duan, V. Chandrasekhar, J. Chen, J. Lin, Z. Wang, T. Huang, B. Girod, and W. Gao, "Overview of the mpeg-cdvs standard," *IEEE Transactions on Image Processing*, vol. 25, no. 1, pp. 179–194, 2015.
- [2] L.-Y. Duan, Y. Lou, Y. Bai, T. Huang, W. Gao, V. Chandrasekhar, J. Lin, S. Wang, and A. C. Kot, "Compact descriptors for video analysis: The emerging mpeg standard," *IEEE MultiMedia*, vol. 26, no. 2, pp. 44–54, 2018.
- [3] L. Duan, J. Liu, W. Yang, T. Huang, and W. Gao, "Video coding for machines: A paradigm of collaborative compression and intelligent analytics," *IEEE Transactions on Image Processing*, vol. 29, pp. 8680–8695, 2020.
- [4] S. Xia, K. Liang, W. Yang, L. Yu Duan, and J. Liu, "An emerging coding paradigm vcm: A scalable coding approach beyond feature and signal," *2020 IEEE International Conference on Multimedia and Expo (ICME)*, pp. 1–6, 2020.
- [5] X. Jin, R. Feng, S. Sun, R. Feng, T. He, and Z. Chen, "Semantically video coding: Instill static-dynamic clues into structured bitstream for ai tasks," *arXiv preprint arXiv:2201.10162*, 2022.
- [6] S. Sun, T. He, and Z. Chen, "Semantic structured image coding framework for multiple intelligent applications," *IEEE Transactions on Circuits and Systems for Video Technology*, vol. 31, no. 9, pp. 3631–3642, 2020.
- [7] G. Lu, X. Zhang, W. Ouyang, L. Chen, Z. Gao, and D. Xu, "An end-to-end learning framework for video compression," *IEEE Transactions on Pattern Analysis and Machine Intelligence*, 2020.
- [8] J. Lin, D. Liu, H. Li, and F. Wu, "M-LVC: Multiple frames prediction for learned video compression," in *Proceedings of the IEEE/CVF Conference on Computer Vision and Pattern Recognition (CVPR)*, 2020, pp. 3546–3554.
- [9] Z. Hu, D. Xu, G. Lu, W. Jiang, W. Wang, and S. Liu, "Fvc: An end-to-end framework towards deep video compression in feature space," *IEEE Transactions on Pattern Analysis and Machine Intelligence*, 2022.
- [10] J. Li, B. Li, and Y. Lu, "Deep contextual video compression," *Advances in Neural Information Processing Systems*, vol. 34, pp. 18 114–18 125, 2021.
- [11] X. Sheng, J. Li, B. Li, L. Li, D. Liu, and Y. Lu, "Temporal context mining for learned video compression," *IEEE Transactions on Multimedia*, 2022.
- [12] Y. Shi, Y. Ge, J. Wang, and J. Mao, "AlphaVC: High-performance and efficient learned video compression," in *European Conference on Computer Vision (ECCV)*. Springer, 2022, pp. 616–631.
- [13] Y.-H. Ho, C.-P. Chang, P.-Y. Chen, A. Gnutti, and W.-H. Peng, "CANF-VC: Conditional augmented normalizing flows for video compression," *European Conference on Computer Vision (ECCV)*, vol. 13676, pp. 207–223, 2022.
- [14] J. Li, B. Li, and Y. Lu, "Hybrid spatial-temporal entropy modelling for neural video compression," in *Proceedings of the 30th ACM International Conference on Multimedia*, 2022, pp. 1503–1511.
- [15] Z. Chen, K. Fan, S. Wang, L. Duan, W. Lin, and A. C. Kot, "Intermediate deep feature compression: Toward intelligent sensing," *IEEE transactions on image processing : a publication of the IEEE Signal Processing Society*, September 2019.
- [16] Y. Zhang, M. Rafie, and S. Liu, "Use cases and requirements for video coding for machines," *ISO/IEC JTC*, vol. 1, 2021.
- [17] C.-Y. Wu, N. Singhal, and P. Krahenbuhl, "Video compression through image interpolation," in *Proceedings of the European Conference on Computer Vision (ECCV)*, 2018, pp. 416–431.
- [18] J. Liu, S. Wang, W.-C. Ma, M. Shah, R. Hu, P. Dhawan, and R. Urtasun, "Conditional entropy coding for efficient video compression," in *European Conference on Computer Vision (ECCV)*. Springer, 2020, pp. 453–468.
- [19] F. Mentzer, G. Toderici, D. Minnen, S.-J. Hwang, S. Caelles, M. Luccic, and E. Agustsson, "Vct: A video compression transformer," *arXiv preprint arXiv:2206.07307*, 2022.
- [20] A. Habibiyan, T. v. Rozendaal, J. M. Tomczak, and T. S. Cohen, "Video compression with rate-distortion autoencoders," in *Proceedings of the IEEE/CVF International Conference on Computer Vision (ICCV)*, October 2019.
- [21] W. Sun, C. Tang, W. Li, Z. Yuan, H. Yang, and Y. Liu, "High-quality single-model deep video compression with frame-conv3d and multi-frame differential modulation," in *European Conference on Computer Vision (ECCV)*. Springer, 2020, pp. 239–254.
- [22] G. J. Sullivan, J.-R. Ohm, W.-J. Han, and T. Wiegand, "Overview of the high efficiency video coding (HEVC) standard," *IEEE Transactions on circuits and systems for video technology*, vol. 22, no. 12, pp. 1649–1668, 2012.
- [23] T. Wiegand, G. J. Sullivan, G. Bjontegaard, and A. Luthra, "Overview of the H.264/AVC video coding standard," *IEEE Transactions on Circuits and Systems for Video Technology*, vol. 13, no. 7, pp. 560–576, 2003.
- [24] B. Bross, Y.-K. Wang, Y. Ye, S. Liu, J. Chen, G. J. Sullivan, and J.-R. Ohm, "Overview of the versatile video coding (VVC) standard and its applications," *IEEE Transactions on Circuits and Systems for Video Technology*, 2021.
- [25] A. Ranjan and M. J. Black, "Optical flow estimation using a spatial pyramid network," in *Proceedings of the IEEE/CVF Conference on Computer Vision and Pattern Recognition (CVPR)*, 2017, pp. 4161–4170.
- [26] E. Ilg, N. Mayer, T. Saikia, M. Keuper, A. Dosovitskiy, and T. Brox, "FlowNet 2.0: Evolution of optical flow estimation with deep networks," in *Proceedings of the IEEE conference on computer vision and pattern recognition (CVPR)*, 2017, pp. 2462–2470.
- [27] J. Ballé, V. Laparra, and E. P. Simoncelli, "End-to-end optimized image compression," in *International Conference on Learning Representations, (ICLR) 2017, Toulon, France, April 24–26, 2017, Conference Track Proceedings*, 2017.
- [28] J. Ballé, D. Minnen, S. Singh, S. J. Hwang, and N. Johnston, "Variational image compression with a scale hyperprior," in *International Conference on Learning Representations (ICLR)*, 2018.
- [29] M. Tassano, J. Delon, and T. Veit, "Fastdvdnet: Towards real-time deep video denoising without flow estimation," in *Proceedings of*

- the IEEE/CVF Conference on Computer Vision and Pattern Recognition (CVPR), 2020, pp. 1354–1363.
- [30] X. Xia and B. Kulis, “W-net: A deep model for fully unsupervised image segmentation,” *arXiv preprint arXiv:1711.08506*, 2017.
 - [31] J. Hu, L. Shen, S. Albanie, G. Sun, and E. Wu, “Squeeze-and-excitation networks,” *IEEE Transactions on Pattern Analysis and Machine Intelligence*, vol. 42, no. 8, pp. 2011–2023, 2020.
 - [32] M. Tassano, J. Delon, and T. Veit, “Dvdnet: A fast network for deep video denoising,” in *2019 IEEE International Conference on Image Processing (ICIP)*, 2019, pp. 1805–1809.
 - [33] J. Lin, C. Gan, K. Wang, and S. Han, “Tsm: Temporal shift module for efficient and scalable video understanding on edge devices,” *IEEE Transactions on Pattern Analysis and Machine Intelligence*, 2020.
 - [34] K. He, X. Zhang, S. Ren, and J. Sun, “Deep residual learning for image recognition,” in *Proceedings of the IEEE Conference on Computer Vision and Pattern Recognition (CVPR)*, 2016, pp. 770–778.
 - [35] S. Ren, K. He, R. Girshick, and J. Sun, “Faster r-cnn: Towards real-time object detection with region proposal networks,” *IEEE Transactions on Pattern Analysis and Machine Intelligence*, vol. 39, no. 6, pp. 1137–1149, 2017.
 - [36] H. Wu, Y. Chen, N. Wang, and Z. Zhang, “Sequence level semantics aggregation for video object detection,” in *Proceedings of the IEEE/CVF International Conference on Computer Vision (ICCV)*, 2019, pp. 9217–9225.
 - [37] T. Xue, B. Chen, J. Wu, D. Wei, and W. T. Freeman, “Video enhancement with task-oriented flow,” *International Journal of Computer Vision*, vol. 127, no. 8, pp. 1106–1125, 2019.
 - [38] F. Perazzi, J. Pont-Tuset, B. McWilliams, L. Van Gool, M. Gross, and A. Sorkine-Hornung, “A benchmark dataset and evaluation methodology for video object segmentation,” in *Proceedings of the IEEE Conference on Computer Vision and Pattern Recognition (CVPR)*, 2016, pp. 724–732.
 - [39] S. Nah, S. Baik, S. Hong, G. Moon, S. Son, R. Timofte, and K. Mu Lee, “Ntire 2019 challenge on video deblurring and super-resolution: Dataset and study,” in *Proceedings of the IEEE/CVF Conference on Computer Vision and Pattern Recognition Workshops*, 2019, pp. 0–0.
 - [40] K. Soomro, A. R. Zamir, and M. Shah, “UCF101: A dataset of 101 human actions classes from videos in the wild,” *arXiv preprint arXiv:1212.0402*, 2012.
 - [41] H. Idrees, A. R. Zamir, Y.-G. Jiang, A. Gorban, I. Laptev, R. Sukthankar, and M. Shah, “The thumos challenge on action recognition for videos “in the wild,”” *Computer Vision and Image Understanding*, vol. 155, pp. 1–23, 2017.
 - [42] O. Russakovsky, J. Deng, H. Su, J. Krause, S. Satheesh, S. Ma, Z. Huang, A. Karpathy, A. Khosla, M. Bernstein *et al.*, “Imagenet large scale visual recognition challenge,” *International Journal of Computer Vision*, vol. 115, no. 3, pp. 211–252, 2015.
 - [43] X. Zhu, Y. Wang, J. Dai, L. Yuan, and Y. Wei, “Flow-guided feature aggregation for video object detection,” in *Proceedings of the IEEE International Conference on Computer Vision (ICCV)*, 2017, pp. 408–417.
 - [44] A. Mercat, M. Viitanen, and J. Vanne, “Uvg dataset: 50/120fps 4k sequences for video codec analysis and development,” in *Proceedings of the 11th ACM Multimedia Systems Conference*, 2020, pp. 297–302.
 - [45] H. Wang, W. Gan, S. Hu, J. Y. Lin, L. Jin, L. Song, P. Wang, I. Katsavounidis, A. Aaron, and C.-C. J. Kuo, “MCL-JCV: a jnd-based H.264/AVC video quality assessment dataset,” in *2016 IEEE international conference on image processing (ICIP)*. IEEE, 2016, pp. 1509–1513.
 - [46] F. David, S. Karl, and R. Chris, “Doc. JCTVC-N1006: Common test conditions and software reference configurations for HEVC range extensions,” *Joint Collaborative Team on Video Coding (JCT-VC) of ITU-T SG*, 2013.
 - [47] X. Wang, K. C. Chan, K. Yu, C. Dong, and C. Change Loy, “Edvr: Video restoration with enhanced deformable convolutional networks,” in *Proceedings of the IEEE/CVF Conference on Computer Vision and Pattern Recognition Workshops*, 2019, pp. 0–0.
 - [48] C. Liu and D. Sun, “On bayesian adaptive video super resolution,” *IEEE Transactions on Pattern Analysis and Machine Intelligence*, vol. 36, no. 2, pp. 346–360, 2013.
 - [49] I. Loshchilov and F. Hutter, “Decoupled weight decay regularization,” in *International Conference on Learning Representations (ICLR)*, 2019.
 - [50] Z. Wang, E. P. Simoncelli, and A. C. Bovik, “Multiscale structural similarity for image quality assessment,” in *The Thrity-Seventh Asilomar Conference on Signals, Systems & Computers*, 2003, vol. 2. Ieee, 2003, pp. 1398–1402.
 - [51] MMAction2 Contributors, “Openmmlab’s next generation video understanding toolbox and benchmark,” <https://github.com/open-mmlab/mmdetection>, 2020.
 - [52] MMTracking Contributors, “MMTracking: OpenMMLab video perception toolbox and benchmark,” <https://github.com/open-mmlab/mmdetection>, 2020.
 - [53] G. Vaksman, M. Elad, and P. Milanfar, “Patch craft: Video denoising by deep modeling and patch matching,” in *Proceedings of the IEEE/CVF International Conference on Computer Vision (ICCV)*, 2021, pp. 2157–2166.
 - [54] C. Huang, J. Li, B. Li, D. Liu, and Y. Lu, “Neural compression-based feature learning for video restoration,” in *Proceedings of the IEEE/CVF Conference on Computer Vision and Pattern Recognition (CVPR)*, 2022, pp. 5872–5881.
 - [55] Y. Tian, Y. Zhang, Y. Fu, and C. Xu, “Tdan: Temporally-deformable alignment network for video super-resolution,” in *Proceedings of the IEEE/CVF Conference on Computer Vision and Pattern Recognition (CVPR)*, 2020, pp. 3360–3369.
 - [56] W. Li, X. Tao, T. Guo, L. Qi, J. Lu, and J. Jia, “Mucan: Multi-correspondence aggregation network for video super-resolution,” in *European Conference on Computer Vision (ECCV)*. Springer, 2020, pp. 335–351.
 - [57] C. Feichtenhofer, H. Fan, J. Malik, and K. He, “Slowfast networks for video recognition,” in *Proceedings of the IEEE/CVF International Conference on Computer Vision (ICCV)*, 2019, pp. 6202–6211.
 - [58] D. Tran, L. Bourdev, R. Fergus, L. Torresani, and M. Paluri, “Learning spatiotemporal features with 3d convolutional networks,” in *Proceedings of the IEEE International Conference on Computer Vision (ICCV)*, 2015, pp. 4489–4497.
 - [59] J. Carreira and A. Zisserman, “Quo vadis, action recognition? a new model and the kinetics dataset,” in *proceedings of the IEEE Conference on Computer Vision and Pattern Recognition (CVPR)*, 2017, pp. 6299–6308.
 - [60] X. Zhu, Y. Xiong, J. Dai, L. Yuan, and Y. Wei, “Deep feature flow for video recognition,” in *Proceedings of the IEEE conference on Computer Vision and Pattern Recognition (CVPR)*, 2017, pp. 2349–2358.
 - [61] T. Mallikarachchi, D. Talagala, H. Kodikara Arachchi, C. Hewage, and A. Fernando, “A decoding-complexity and rate-controlled video-coding algorithm for HEVC,” *Future Internet*, vol. 12, no. 7, p. 120, 2020.